

Article

Provenance of Detrital Rutiles from the Triassic–Jurassic Sandstones in Franz Josef Land (Barents Sea Region, Russian High Arctic): U–Pb Ages and Trace Element Geochemistry

Victoria Ershova ^{1,2,3,*} , Andrei Prokopiev ³  and Daniel Stockli ⁴

¹ Institute of Earth Sciences, Saint Petersburg State University, Universitetskaya nab. 7/9, St. Petersburg 199034, Russia

² Geological Institute of Russian Academy of Sciences, Pyzhevski Lane 7, Moscow 119017, Russia

³ Diamond and Precious Metal Geology Institute, Siberian Branch, Russian Academy of Sciences, Lenin av. 39, Yakutsk 677000, Russia; prokopiev@diamond.ysn.ru

⁴ Department of Geological Sciences, Jackson School of Geoscience, University of Texas at Austin, Austin, TX 78712-1692, USA; stockli@jsg.utexas.edu

* Correspondence: v.ershova@spbu.ru

Abstract: Provenance study plays an important role in paleogeographic and tectonic reconstructions. Detrital zircons are commonly used to identify sediment provenance; however, a wide range of detrital zircon ages in clastic rock often represent a fingerprint of reworked older terrigenous successions rather than ages of magmatism and metamorphism in the provenance area. This study focuses on the provenance of detrital rutile grains in the Triassic–Jurassic sandstones from Franz Josef Land and shows the importance of multiproxy approaches for provenance studies. Trace element data demonstrate that most rutile grains were sourced from metapelitic rocks, with a subordinate population having a metamafic origin. The Zr-in-rutile thermometer and U–Pb geochronology suggest that detrital rutile grains were predominantly derived from rocks that underwent amphibolite facies metamorphism during the Paleozoic era, with a predominance of the Carboniferous–Permian ages. Therefore, we suggest that the provenance area for the studied sandstones on Franz Josef Land has a similar geological history to the Taimyr region and Severnaya Zemlya archipelago. We propose that this crustal domain extends across the Kara Sea and forms the basement to the north and east of FJL, representing a proximal provenance for the studied Mesozoic terrigenous rocks. This domain experienced both Middle–Late Ordovician and Carboniferous–Permian metamorphism. The comparison of U–Pb dating and the geochemistry of rutile, U–Th/He, and U–Pb dating of zircons showed that detrital rutiles are the powerful tool in provenance restoration and can give additional constraints when a provenance area locates within collisional–convergent settings.

Keywords: detrital rutile; sandstone provenance; U–Pb geochronology; Franz Josef Land; Barents Sea; Arctic



Citation: Ershova, V.; Prokopiev, A.; Stockli, D. Provenance of Detrital Rutiles from the Triassic–Jurassic Sandstones in Franz Josef Land (Barents Sea Region, Russian High Arctic): U–Pb Ages and Trace Element Geochemistry. *Geosciences* **2024**, *14*, 41. <https://doi.org/10.3390/geosciences14020041>

Academic Editors: Jesus Martinez-Frias and Angelos G. Maravelis

Received: 9 December 2023

Revised: 19 January 2024

Accepted: 23 January 2024

Published: 3 February 2024



Copyright: © 2024 by the authors. Licensee MDPI, Basel, Switzerland. This article is an open access article distributed under the terms and conditions of the Creative Commons Attribution (CC BY) license (<https://creativecommons.org/licenses/by/4.0/>).

1. Introduction

There has been a significant increase in the interest of reconstructing the geological history of sedimentary basins using isotope–geochronological, isotope–geochemical and thermochronological methods in recent years. Clastic rocks, especially sandstone, are widely distributed in various depositional environments implying their usability in diverse fundamental and applied research [1–3]. The U–Pb dating of detrital zircons has become a routine method for provenance studies of clastic rocks [4–6]. This is largely due to the high content of zircon grains in the heavy fraction of sandstones, a well-established dating technique, and the presence of numerous laboratories around the world for analytical work. At the same time, zircons also contain a number of features that complicate the reconstruction of clastic provenances, if these are the sole archives used. The main complication involves

the potential for zircons to undergo repeated reworking during the sedimentary processes. Therefore, a wide range of detrital zircon ages in a clastic rock often represents a fingerprint of reworked older terrigenous successions, as opposed to the ages of magmatism and metamorphism in the provenance area [7–11]. Moreover, zircons are usually sourced from felsic magmatic rocks and high-grade metamorphic rocks but are rare in mafic magmatic rocks [4,5,12].

To overcome these difficulties, analytical methods have been developed for dating other minerals which are less prone to multiple phases of reworking by sedimentary processes and/or are formed in a wider range of parent rocks, such as apatites, monazite, rutiles, and titanites, among others [13–15]. Detrital rutiles are of particular interest, as they can not only be dated by the U-Pb (LA-ICP-MS) method, but rare earth and trace element concentrations can also be used as indicators of the composition and the metamorphic grade of the provenance area [16–18]. Therefore, detrital zircon and rutile minerals can yield different, but complementary insights for provenance studies. Detrital U-Pb zircon ages mainly provide evidence for magmatic, and to a lesser extent, high-grade metamorphic events, whereas rutiles commonly form in relatively high-grade metamorphic facies (e.g., [18,19]). Furthermore, detrital rutiles, in contrast to zircons, have a significantly lower closure temperature for Pb (500–650 °C) [20–22]. Rutiles are not only sensitive to tectonic and metamorphic processes, but they also have the additional advantage of being common in both metapelitic and metamafic rocks. The usefulness of rutiles in provenance studies has been proven by numerous researchers [18,23–28]. In these studies, U-Pb dating of rutiles has been used to derive the age of upper amphibolite to lower granulite facies metamorphic events within the provenance area. In addition, trace element compositions of detrital rutiles provide information on the provenance rock composition and temperature conditions of metamorphism.

In this study, we generated U-Pb age data and trace element composition of detrital rutiles from three Triassic–Jurassic sandstone samples from Franz Josef Land (FJL; north-eastern Barents Sea). We constrain the rock composition found in the provenance area, along with the degree and timing of metamorphism, to create a more in-depth reconstruction of the provenance of the studied sediments and their transport directions. This study yields the first detrital rutile U-Pb ages and trace element chemistry from Mesozoic sandstones of the entire Barents Sea region.

In addition, we show how the age distribution of detrital rutiles apply to the reconstruction of the tectonic settings at the time of deposition, complementing and refining interpretations based solely on detrital zircons.

2. Geological Background

FJL represents the uplifted north-eastern part of the Barents Sea shelf, representing a rare window into the Mesozoic succession of the area (Figures 1–3). The Barents continental shelves supposedly comprise Neoproterozoic and Early–Middle Paleozoic basement domains [29–32]. The pre-Mesozoic stratigraphic framework of FJL is based on the stratigraphy penetrated by the deep Nagurskaya well, drilled on Alexandra Land Island in the westernmost part of the archipelago [33–35], along with a detailed studied of the conglomerates containing reworked clasts of older stratigraphy in the south-eastern part of FJL [36].

Precambrian rocks comprise intensely deformed quartz mica schists and phyllites, overlain above an angular unconformity by sub-horizontally bedded clastic-carbonate Carboniferous succession [34,35]. The Triassic to Cretaceous clastic succession is exposed across FJL and intruded or overlain by late Early Cretaceous mafic dykes, sills, and basalts, attributed to the High Arctic Large Igneous Province (HALIP) [37–39] (Figures 2 and 3). The correlation of the different Mesozoic sedimentary units across FJL is debated [35,40,41]. Here, we mainly follow the stratigraphic scheme of [35,40] due to its applicability for the whole archipelago.

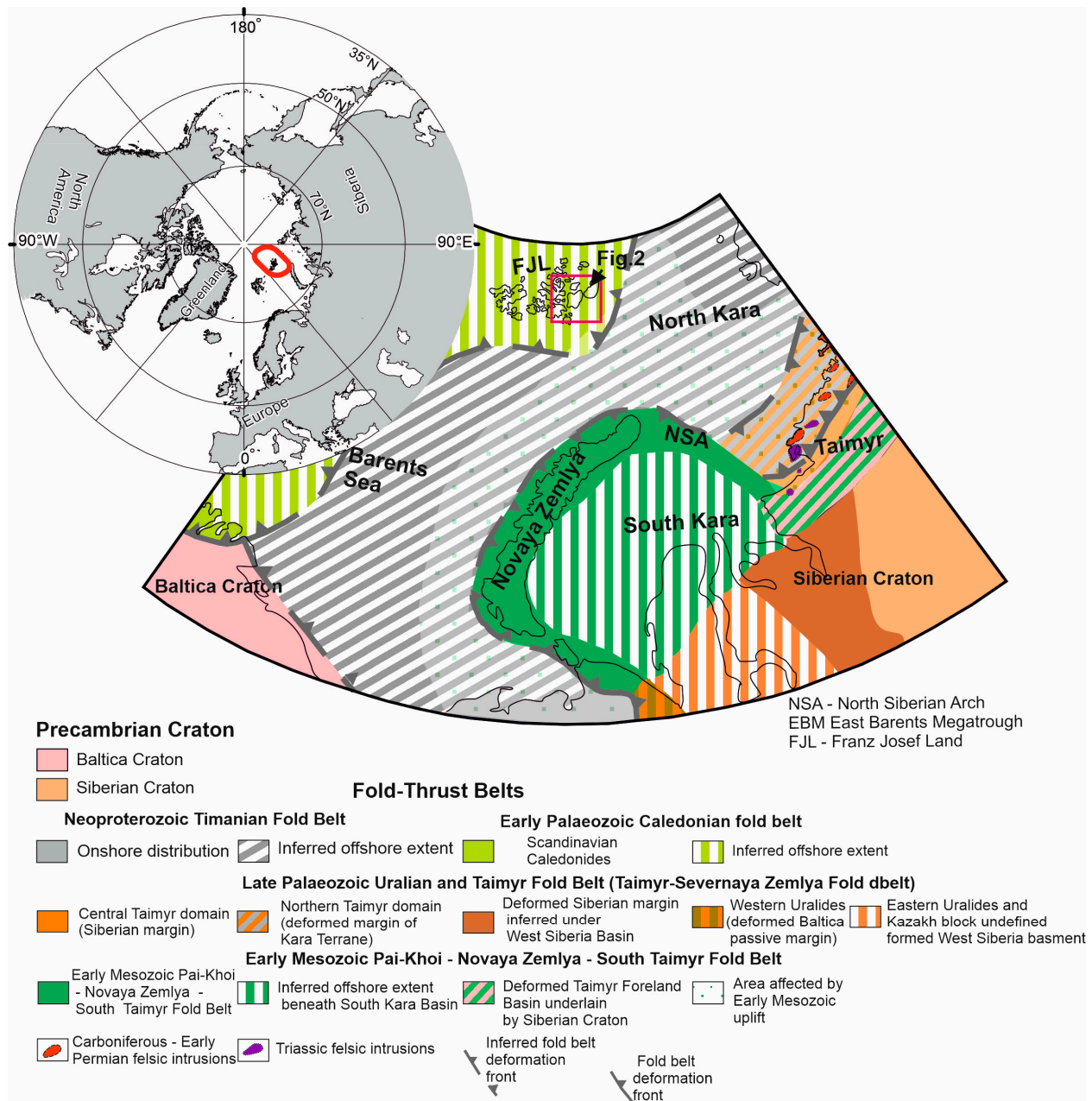


Figure 1. Simplified tectonic map of study region modified after [29,30,32]. The red rectangle shows the area of Figure 2.

The Induan–Norian succession (Belozemel, Matusevich, Ermakov, Graham Bell and Heiss formations) disconformably overlies Carboniferous succession in the Nagurskaya well. The Triassic strata comprise alternating argillites, sandstones, and siltstones, with subordinate beds of clayey limestones reaching a thickness of 3500 m. The Vasilev Formation (Rhaetian; 100–370 m in thickness) comprises polymictic sandstones and sands with beds of conglomerates and gritstones, along with rare beds of siltstones and argillites [35,40]. A markable hiatus occurred between Norian and Rhaetian deposits across FJL [42].

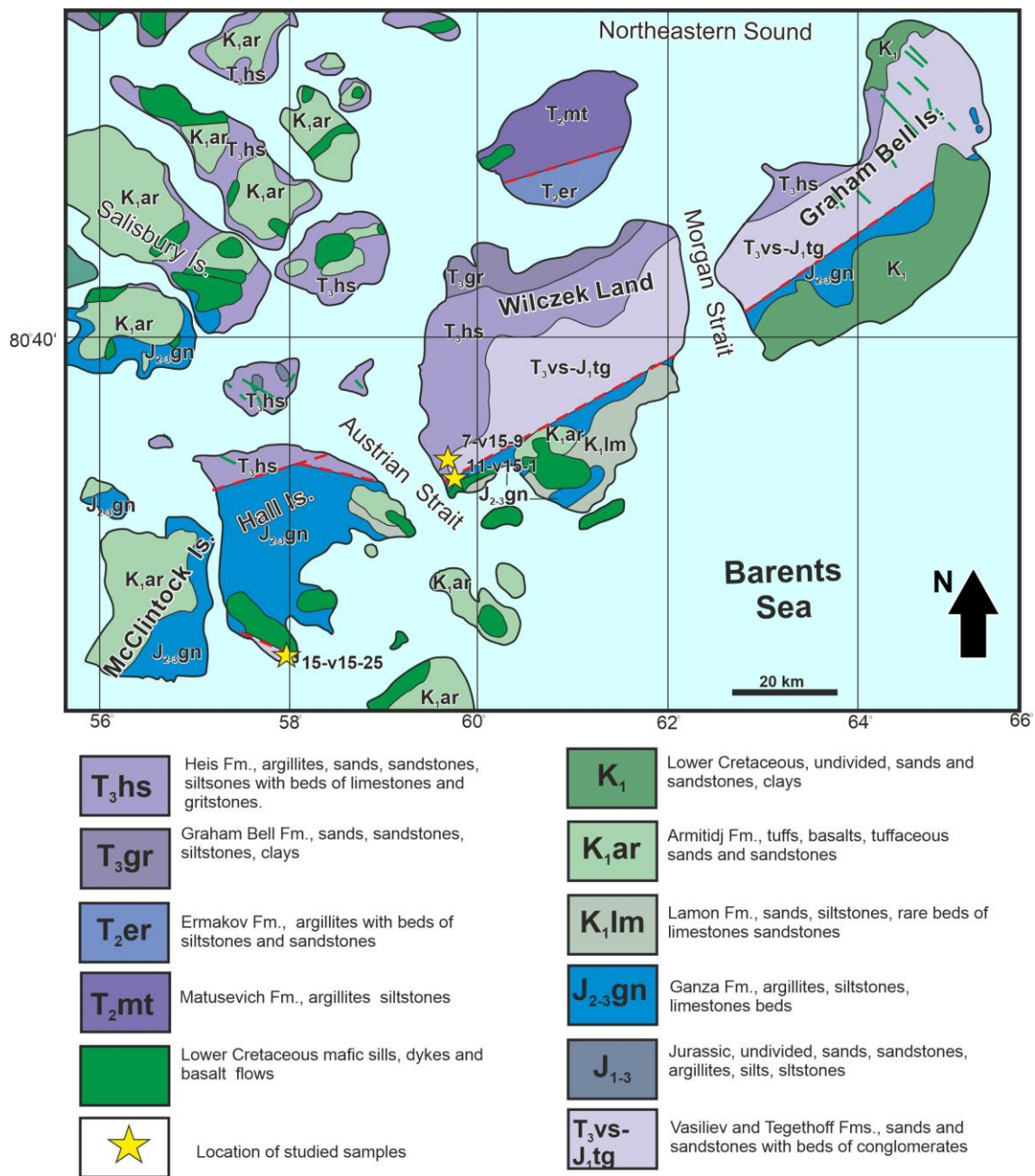


Figure 2. Simplified geological map of southern part of FJL with location of dated samples (simplified modified after [35,40]).

The Tegethoff Formation (Hettangian–Lower Toarcian; 60–350 m in thickness) unconformably overlies upper Triassic succession and mainly comprises coarse- to medium-grained polymictic sands and sandstones, gritstones and conglomerate beds, with occasional thin silt beds [35,40]. The Ganza Formation (Toarcian–Volgian; 40–270 m in thickness) has a patchy distribution across the archipelago due to subsequent early Cretaceous erosion. It mainly comprises alternating argillites and siltstones with occasional units of clayey limestone and rare beds of sandstone. The Lamon Formation (Oxfordian–Valanginian) comprises sandstones and sands with beds of siltstone and argillite [35,40,41].

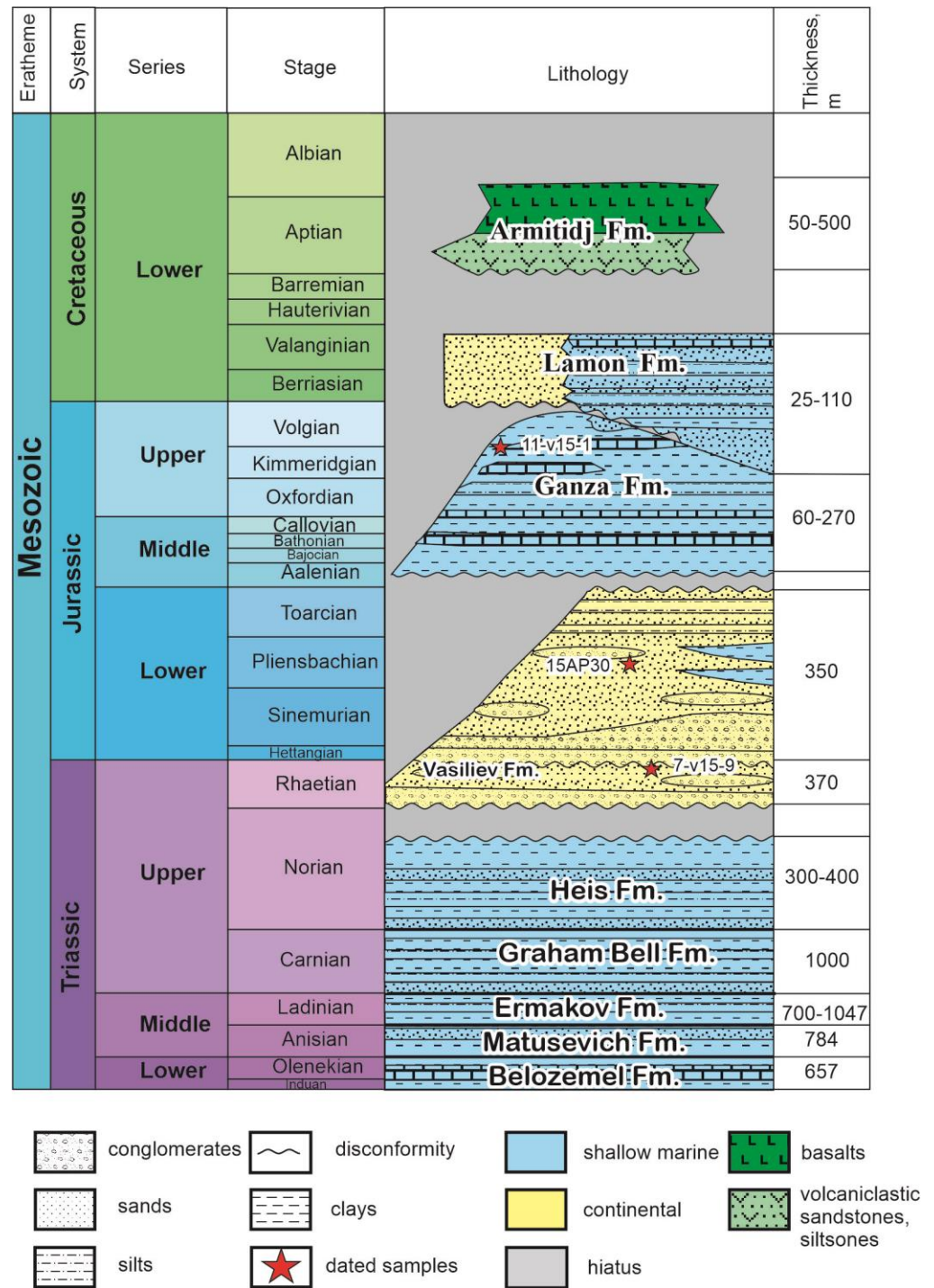


Figure 3. Simplified stratigraphic chart of Mesozoic strata of FJL (compiled from [33,35,40–42]). The major unconformities are pre-Rhaetian, pre-Aalenian, pre-Aptian.

The Armitidj Formation (Hauterivian (?)-Aptian) unconformably overlies various Triassic–Lower Cretaceous formations, comprising alternating basalts and tuffaceous sandstones. The age of formation is mainly based on the isotopic dating of mafic rocks with ⁴⁰Ar–³⁹Ar dating yielded ages ranging from 189 to 125 Ma [43–47], while the most reliable TIMS U–Pb zircon dates yielded a crystallization age of 122.7 Ma for a thick sill in the Severnaya Well (Graham Bell Island) [37].

3. Materials and Methods

3.1. Geological Position of Dated Samples

Sample 7-v15-9 (Wilczek Land, Ganza Cape area) was collected from outcrops located 3 km to the north-west of the Ganza Cape, where planar and cross-bedded medium- to fine-grained sandstones with rare siltstone layers (Vasiliev Formation; Rhaetian) crop out (Figures 2–4 and Table 1).

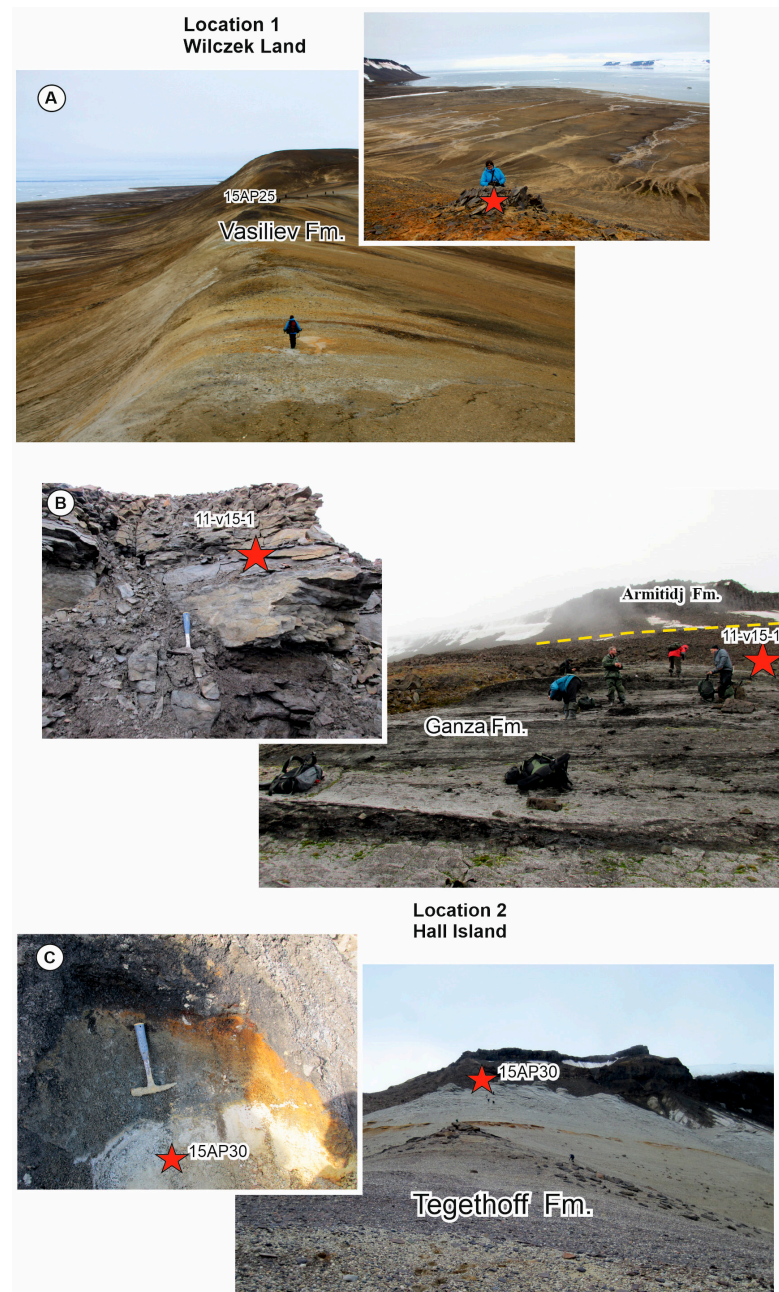


Figure 4. Photo of studied sections and position of dated samples (red stars): (A) Wilczek Land, 3 km to the north-west of Ganza Cape, general view of outcrop of the Vasiliev Fm. (Rhaetian) (left) and the position of 7-v15-9 sample within cross-bedded medium- to fine-grained sandstones, (B) Wilczek Land, 1 km to the north of Ganza Cape, general view of outcrop of the Ganza Fm. (right) and the position of 11-v15-1 sample collected from the sandy siltstone bed (left); (C) Hall Island, Tegethoff Cape, general view of outcrop of the Lower Jurassic Tegethoff Formation (right) and the position of 15AP30 sample within intercalating clays and fine-grained sandstones (left).

Table 1. Summary of locations and compositions of analyzed samples.

Sample Number	Latitude	Longitude	Rock Composition
7-v15-9	N 80°25.563'	E 059°39.570'	Medium-grained polymictic sandstone
11-v15-1	N 80°24.695'	E 059°42.964'	Fine-grained arkosic arenite sandstone
15AP30	N 80°06'13.9"	E 057°53'02.1"	Medium-grained polymictic sandstone

Sample 11-v15-1 was collected from outcrops located 1 km to the north of the Ganza Cape, where black argillites with subordinate thin siltstone layers of the Ganza Formation crop out (Figure 3). The sample has been dated as the latest Kimmeridgian, based on ammonite findings from this locality [25] (Figures 2–4 and Table 1).

Sample 15AP30 (Hall Island, Tegethoff Cape) was collected from the intercalating clays and fine-grained sandstones of the Lower Jurassic Tegethoff Formation (Figures 2–4 and Table 1).

3.2. Analytical Techniques

Samples were crushed and the heavy minerals were concentrated using standard techniques. Zircon monofraction were separated following a standard scheme: grinding, sieving into size fractions, passing of the fraction of <0.25 mm through a centrifugal concentrator, electromagnetic treatment of the obtained heavy fraction, and the final treatment of the concentrate with a heavy liquid. All analyses were carried out at the UTChron geochronology facility in the Department of Geosciences at the University of Texas, Austin. The rutile grains were hand-picked from the bulk-heavy mineral separate, mounted in epoxy, and polished for LA-ICP-MS U-Pb analysis. The sample pucks were loaded into a large-volume Helex sample cell and analyzed with a magnet sector, single collector Element2 ICP-MS with a Photon Machines Analyte G.2 excimer laser (Laser source-Advanced Technology Lasers (ATL) in Wermelskirchen, Germany; the frame that the source sits in that contains all the mirrors, lenses, cameras, etc was made by Photon Machines in Bozeman, Montana, United States). Rutile U-Pb analysis was conducted using a 40- μ m spot size. Rutile R10 (1090 ± 0.9 Ma; [48]) was used as a primary reference standard and rutile R19 (489.5 ± 0.9 Ma; [5]) as a secondary reference standard. A primary $^{238}\text{U}/^{206}\text{Pb}$ standard R10 rutile [48] was used to calculate ages and control for fractionation, while a secondary standard R19 rutile [5] provided an independent verification of ages. The data were reduced using the VizualAgeDRS in Iolite [49–51]. Pbc correction was based on the model Pb composition of [52].

A 40- μ m spot size was used for trace element LA-ICP-MS determinations and concentrations were calibrated against the SRM 610 (NIST) reference glass standard. Raw trace element data were reduced using Iolite 3.7 data reduction software and Trace Element_IS [50]. The rutile U-Pb ages were corrected using a ^{208}Pb correction [15]. Zr-in-rutile crystallization temperatures were calculated using the calibration of [53], with the Tomkins thermometer for a 10 kbar- α -quartz as a default setting, since pressure information is unavailable for detrital rutile grains [17]. Detrital rutile U-Pb analytical results are provided in Table S1.

4. Results

The most frequent rutile grains are dark yellowish to reddish brown. The crystal size is variable and, on average, ranges from approximately 70 μ m to 250 μ m. Most rutile grains are angular, subangular, or subrounded in shape.

4.1. Detrital Rutile Geochemistry

Trace element concentrations of 209 rutile grains from the three sandstone samples were measured and the results are listed in Table S2.

4.1.1. Sample 7-v15-9

Detrital rutile Cr and Nb concentrations exhibit large variations (Cr: 3.7–4918 ppm, Nb: 26–8320 ppm), with all of the grains plotted on the Cr-Nb diagram of [17]. Based on this diagram (Figure 4), about 80% of the detrital rutiles were sourced from metapelitic rocks and 20% from metamafic rocks. A Zr concentration of detrital rutiles ranges from 15.29 to 3718 ppm. The temperatures calculated for detrital rutiles in sample 7-v15-9 range between 464 °C and 902 °C (Figure 5).

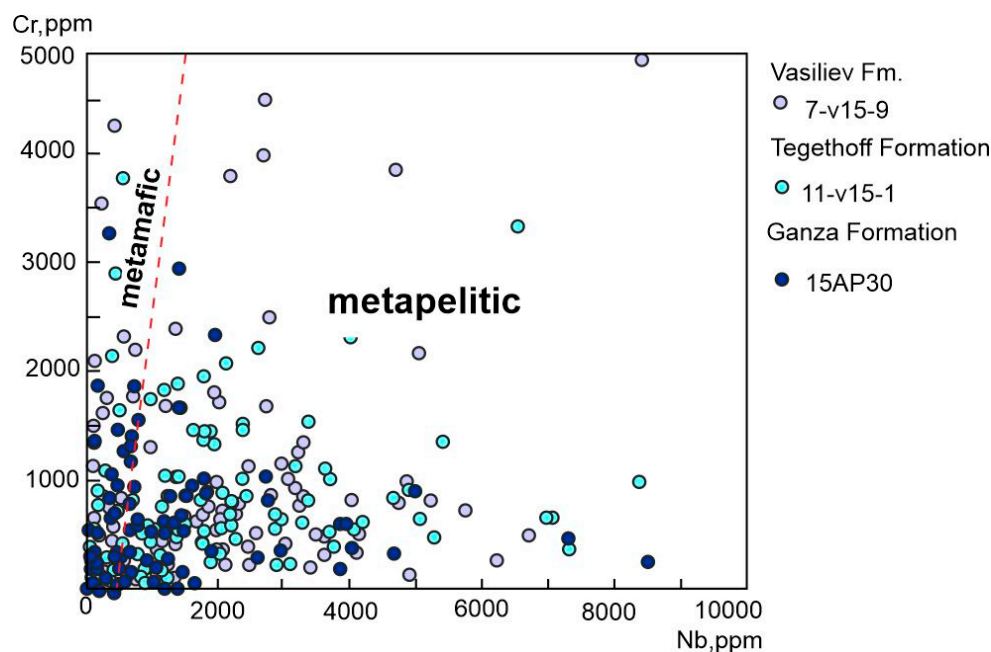


Figure 5. Cr–Nb source rock classification of rutile. Metamafic and metapelitic rutile are discriminated following [17].

4.1.2. Sample 15AP30

Detrital rutile Cr and Nb concentrations also exhibit large variations (Cr: 6–5582 ppm, Nb: 7–8500 ppm). Based on the Cr-Nb diagram (Figure 5), about 70% of the detrital rutiles originated from metapelitic rocks and 30% originated from metamafic rocks. The Zr concentration of detrital rutiles range from 21 to 5100 ppm. The rutile grains yielded temperatures between 481 °C and 943 °C. This temperature distribution suggests that most grains were sourced from amphibolite-facies metamorphic rocks, while only a few were derived from greenschist or granulite-facies metamorphic rocks (Figure 5).

4.1.3. Sample 11-V15-11

The detrital rutile Cr and Nb concentrations also exhibit large variations (Cr: 9–3709 ppm, Nb: 8–8390 ppm). Based on the Cr-Nb diagram (Figure 5), about 87% of the detrital rutiles were transported from metapelitic rocks and 13% from metamafic rocks. The Zr concentration of detrital rutiles range from 23 to 16,000 ppm. The calculated rutile formation temperatures for the detrital rutile grains range between 485 °C and 1122 °C. This temperature distribution suggests that most grains originated from amphibolite-facies metamorphic rocks, while only 20 grains were derived from greenschist or granulite-facies rocks (Figure 6).

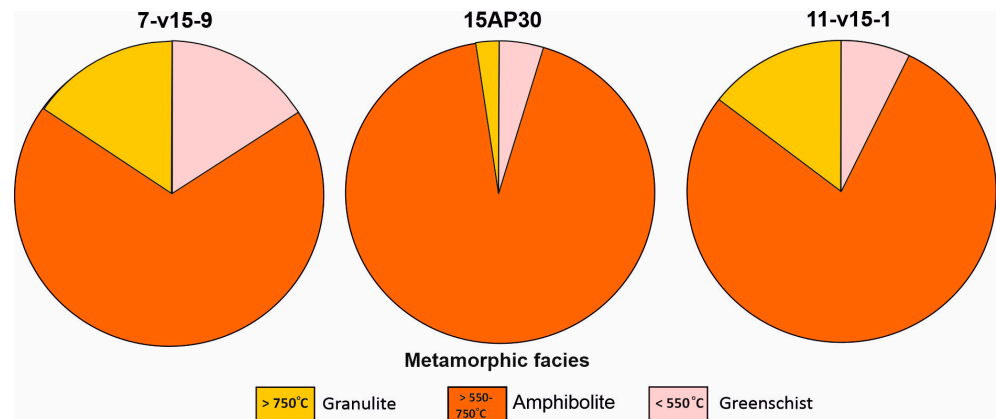


Figure 6. Pie charts showing the percentage of different metamorphic facies for the source rocks within the provenance area of detrital rutile, according to calculated formation temperatures. Metamorphic facies boundaries have been taken from the lower pressure end of facies diagram defined by [54].

4.2. U-Pb Dating of Rutile

4.2.1. Sample 7-v15-9

Most of the dated rutiles are Paleozoic in age (82%). Permian and Carboniferous rutiles are abundant, and comprise 33% of the dated population, forming multiple peaks at ca. 270 and 300–350 Ma. Devonian rutiles (28%) group at ca. 380–400 Ma. Silurian and Ordovician grains together comprise 13% of the dated population and group at ca. 440 and 490 Ma. Precambrian grains (18%) do not form any prominent peaks (Figure 7).

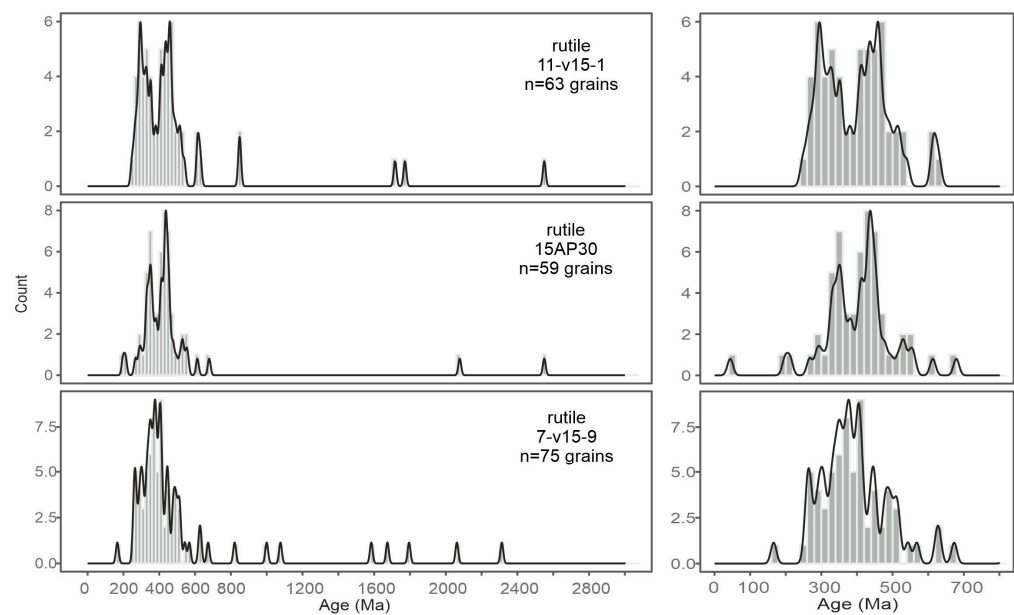


Figure 7. Kernel Density Estimation (KDE) plots depict the U-Pb detrital rutile data from the Upper Triassic (7-v15-9), Lower Jurassic (15AP30) and Upper Jurassic (11-v15-1) samples analyzed in this paper. The age distribution since the 700 Ma was zoomed in the right part of figure. n = number of detrital rutile analyses.

4.2.2. Sample 15AP30

Permian and Carboniferous rutiles comprise 27% of the dated population and form peaks at ca. 330 and 350 Ma. Devonian rutiles comprise 21% of the dated grains and form a subordinate peak at 390 Ma. Silurian, Ordovician, and Cambrian rutiles together comprise 37% of the population and form peaks at ca. 400, 430 and 459 Ma. Precambrian rutiles (10%) do not form any significant peaks (Figure 7).

4.2.3. Sample 11-V15-1

Most of the dated rutiles are Paleozoic in age (83%), with Permian rutiles (24%) forming peaks at ca. 250 and 295 Ma. The Carboniferous rutiles comprise 19% of the dated population and group at ca. 300–310 and 340–350 Ma. The Devonian–Cambrian zircons (39%) form multiple peaks at ca. 380–400 and 430–450 Ma. Precambrian zircons (16%) do not form reliable groups (Figure 7).

5. Provenance Interpretation

5.1. Previous Provenance Study

A previous provenance study of the Triassic–Cretaceous strata on FJL on the same samples was based on the U–Pb and (U–Th)/He dating of detrital zircons [36]. Detrital zircon U–Pb dating revealed that Triassic grains form a small peak at 220–230 Ma. Most of the dated zircons (54–66%) are Paleozoic in age, with a predominance of Permian and Carboniferous grains grouping at ca. 250, 295, 300–310 and 340–350 Ma. Devonian–Ordovician zircons mainly group at ca. 380–400 and 430–450 Ma. Precambrian zircons form subordinate peaks mainly between 550–650, 800–1000 and 1700–1800 Ma.

Detrital zircon (U–Th)/He (ZHe) dating previously [36] was carried out for samples 7-v15-9 and 15AP30. All obtained ZHe ages were older than the depositional ages of the studied deposits, suggesting that these rocks have not been buried deeper than 6–7 km since deposition (assuming a typical continental crust geothermal gradient of 30 °C/km). Therefore, the ZHe ages reflect the timing of exhumation and cooling in the provenance area. A total of eighteen ZHe ages showed a 180–349 Ma age range, with most of these ages grouping at approximately 225 Ma [36].

5.2. Detrital Rutile

Based on the geochemistry of detrital rutiles, most grains were derived from metapelitic rocks with a subordinate rutile population from metamafic rocks (Figure 6). The calculated rutile formation temperatures suggest that most grains were derived from amphibolite-facies metamorphic rocks, with a subordinate number from greenschist and granulite-facies metamorphic rocks. Therefore, based on our geochemical data, we suggest that the provenance area for Mesozoic clastics on FJL was predominantly composed of amphibolite-facies metamorphic rocks.

The distribution of detrital rutile ages within the dated samples is very similar, suggesting a common provenance area for the studied Triassic–Jurassic sedimentary rocks (Figure 7). The few Paleoproterozoic (ca. 1800–1600 Ma) and Mesoproterozoic (1300–1000 Ma) rutile populations can be correlated with magmatic and metamorphic rocks within the basement of the Baltica [55–58]. Neoproterozoic to Cambrian rutiles (650–520 Ma) can be correlated with the main magmatic and metamorphic event within the Timanian orogen, which formed as a result of the latest Neoproterozoic to the earliest Cambrian orogeny along the northeastern margin of Baltica (present day coordinates) ([59,60] and references therein). A prominent detrital rutile population comprising ages between 470 and 420 Ma could be possibly correlated with coeval magmatic and metamorphic events within the Severnaya Zemlya archipelago [61–63].

A Middle–Late Devonian population is prominent in sample 7-v15-9; however, a smaller population of this age can be found in the other samples. A source for the Middle–Late Devonian rutiles is unclear, since coeval metamorphic events have not been documented from onshore. However, Late Devonian mafic magmatism and coeval rifting occurred in northern Novaya Zemlya (Barents Sea region) [64]. Furthermore, significant exhumation of the northern Kara Sea region during the Middle–Late Devonian has been reconstructed from the (U–Th)/He zircon ages [65]. Therefore, we propose that this Middle–Late Devonian tectonism was associated with some metamorphism, forming metamorphic rocks which were a source of the Middle–Late Devonian rutiles in our samples.

The most prominent detrital rutile populations indicate major metamorphic events within the provenance area occurred at ca. 350–320 Ma and again between ca. 280 and

260 Ma. These Late Paleozoic magmatic and tectonic events can be correlated to the Uralian orogeny, formed as a result of a continental collision between Kazakhstan, Siberia, and Laurussia [66–68]. The suture of the Uralian orogeny stretches onshore from the Aral Sea to the Polar Urals, although its northward continuation under the northern West Siberia Basin and further to the north and east are still debated [32,69–72]. However, recent studies pointed out that it continues as far as the Taimyr Peninsula (e.g., [32,71] and references therein). Furthermore, voluminous magmatism and metamorphism occurred between 315 and 288 Ma across northern Taimyr and the southern part of the Severnaya Zemlya archipelago ([71,72] and references therein).

The Upper Triassic and Lower Jurassic strata of FJL comprise a coarse-grained clastic succession with conglomerate beds and were clearly derived from a proximal provenance area. The previous study by [36] proposed that the provenance area for the studied sandstones on Franz Josef Land has a comparable geological history to the Taimyr region and Severnaya Zemlya archipelago, based on the detrital zircon U-Pb dating. They further proposed that this crustal domain extends across the Kara Sea and forms basement to the east and north of FJL, representing a proximal provenance for the studied Mesozoic clastics. Our new detrital rutile data tentatively support this model but in addition, we propose that not only magmatic but also significant metamorphic events affected the provenance area in the Middle–Late Ordovician and Carboniferous–Permian.

5.3. Comparison between U-Pb Dating of Rutiles and Zircons, (U-Th)/He Dating of Zircons and Their Application to Provenance Studies

Since both zircon and rutile are resistant to chemical and physical breakdown, they can be reworked from their host magmatic or metamorphic rocks and preserved as detrital grains within sedimentary rocks. To date, there are thousands of provenance studies based on detrital zircon U-Pb dating, mainly due to well-established analytical techniques. Some of these studies incorporated U-Pb dating of both zircons and rutiles, with even fewer accompanied by an additional geo- or thermochronometer (for example [73]). Here, we compare the data collected from detrital rutiles during this study with previous detrital zircon U-Pb and (U-Th)/He data generated from the same samples by [36], to evaluate the relative merits of the different minerals and analytical approaches for provenance studies (Figure 8).

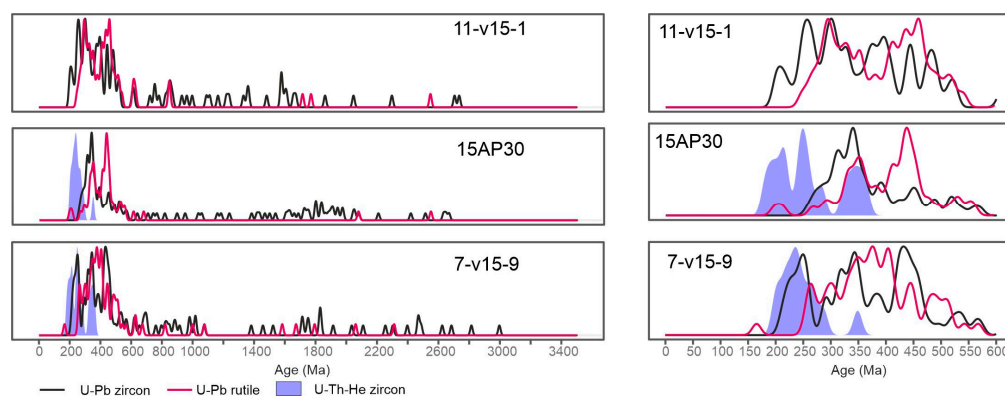


Figure 8. Kernel Density Estimation (KDE) plots depicting the U-Pb detrital rutile and zircon data, as well as ZHe zircon ages from the Upper Triassic Upper Triassic (7-v15-9), Lower Jurassic (15AP30) and Upper Jurassic (11-v15-1) samples analyzed in this paper. Detrital zircon data from [36].

Rutile ages are often characterized by a unimodal distribution, indicative of the youngest metamorphic event(s) within the provenance, while zircons from the same samples often yield a multimodal age distribution, suggesting a significant reworking of older grains. For example, unimodal rutile age distributions have been obtained from the Upper Cretaceous–Eocene strata of western Anatolia [74], Lower Carboniferous flysch of the Istanbul Zone [19], Late Ordovician units from Saxo-Thuringia [75], Precambrian rocks of

central Australia [76], and Cambrian sandstones from Israel and Jordan [77]. Multimodal age spectra are less commonly observed in detrital rutiles, although they have been reported from modern sands of the Mississippi River [78], ice-rafted debris in the North Atlantic [79], and Neogene to recent Himalayan River deposits [27,28]. Moreover, a closer inspection of the data suggests that these non-unimodal age distributions are often better characterized as bimodal rather than multimodal, reflecting either two distinct provenance areas or complex metamorphic events within a single provenance area.

Our comparison of detrital zircon and rutile U-Pb ages suggest that rutiles yield a broadly similar age distribution to detrital zircons for the Mesozoic clastics of FJL. However, Precambrian detrital zircons are more abundant than rutiles, that is possibly explained by the ability of zircon to generally survive the rock cycle from sedimentary to high-grade metamorphic conditions, while rutile usually breakdown at the beginning of the greenschist metamorphic facies and newly forms at upper amphibolite facies conditions [80]. Furthermore, the 470–450 Ma detrital rutile population suggests a significant metamorphic event within the provenance area, yet a significant coeval detrital zircon population of this age is lacking. Therefore, the detrital rutiles clearly highlight a significant metamorphic event which would not have been interpreted from the analysis of detrital zircon U-Pb ages in isolation. The ZHe ages obtained by [36] for two samples (7-v15-9, 15AP30) indicate a significant Late Triassic exhumation event in the provenance area, along with a subordinate Late Paleozoic tectonic event. The Upper Triassic sandstones (sample 7-v15-9) contain Late Triassic ZHe and U-Pb detrital zircon ages but lack rutiles of coeval ages. The integration of all three analytical techniques can be used to suggest that the Late Triassic magmatism and exhumation, based on the detrital zircon ZHe and U-Pb ages, were not accompanied by a significant metamorphism, based on the lack of coeval rutile ages. Lower Jurassic sandstones (sample 15AP30) contain evidence for two pronounced exhumation events of latest Permian and latest Triassic age within the provenance area, but both events were not accompanied by coeval magmatism and metamorphism. The detrital rutile and zircon age spectra of the studied sandstones are both multimodal, suggestive of complex drainage systems supplying clastics from multiple provenance regions, or a single provenance region with a complex geological history involving multiple metamorphic and magmatic events [73].

A comparison of detrital zircon ZHe and U-Pb ages, along with detrital rutile U-Pb ages, suggests that the youngest significant exhumation event occurred during the latest Triassic age within the provenance area. The geodynamic cause of this Triassic/Jurassic tectonic event within the Arctic region is unclear. However, it affected an extensive region encompassing the Taimyr Severnaya Zemlya fold belt, Novaya Zemlya archipelago, and possibly extended across the central part of the Kara Sea [29,81]. Since coeval magmatism and metamorphism have not been reported across the study area, along with an absence of collisional events of this age, this pronounced tectonic event could represent an intracontinental orogen encompassing the Taimyr region and stretching across the central and possibly northern part of the Kara Sea to form the proximal provenance area for studied clastics. Such orogens are comparatively rare in the geological record and are therefore poorly understood [82]. We speculate that the onset of the cooling phase is likely related to far-field propagation and the formation of an intracontinental orogen. Therefore, reconstruction of intracontinental orogens require additional lower temperature constraints beyond the applicability of the detrital rutile and zircon U-Pb dating.

Detrital minerals represent a powerful archive for the reconstruction of the tectonic settings of sedimentary basins and providing an insight into tectonic processes affecting provenance regions. A cumulative proportion distribution against a growth-deposition ages diagram based on detrital zircon ages has been proposed by [4] and applied to detrital rutiles by [24], representing a powerful tool for deciphering tectonic settings of basins and the provenance areas. Therefore, we applied the same approach for our dataset (Figure 9) to demonstrate that both detrital rutile and zircon data plot in the convergent to collisional basin fields. The detrital rutile and zircon cumulative distributions are similar

but not identical, with the large number of Precambrian detrital zircons with ages which have not been reset during the younger tectonic and metamorphic events. Consequently, detrital rutiles appear to be better candidates for reconstructing provenance areas formed in convergent to collisional settings, since younger tectonic events are better preserved compared to detrital zircons. The global database of detrital rutile data generated to date has the potential to yield important information on the reconstruction of tectonic settings within provenance areas and the tectonothermal evolution of provenance areas formed within convergent to collisional geodynamic settings.

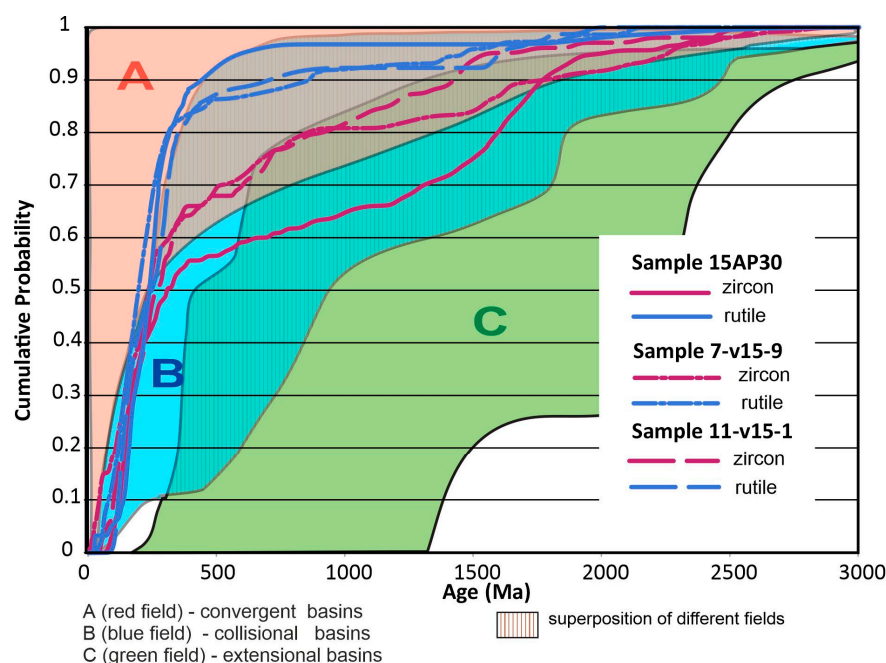


Figure 9. Cumulative proportion distributions against growth-deposition ages diagram, modified from [4]. Colored fields show the different depositional tectonic settings.

6. Conclusions

Cr and Nb concentrations in detrital rutiles show large variations. According to the Cr-Nb diagram, a majority (70–87%) of the detrital rutiles were derived from the metapelithic with subordinate populations from the metamafic rocks (13–30%). The calculated rutile formation temperatures for detrital rutile grains showed that a majority of the detrital rutiles grains were derived from the amphibolite-facies metamorphic rocks, while only a few were derived from greenschist and granulite-facies metamorphic rocks.

Most of the dated grains are Paleozoic in age (77–85%). Permian and Carboniferous rutiles are abundant and comprise the dated population, forming multiple peaks at ca. 270 and 300–350 Ma. Devonian rutiles form a subordinate population at ca. 380–400 Ma. Silurian and Ordovician grains form groups at ca. 440 and 490 Ma. Precambrian grains do not form any significant peaks. Thus, the provenance area of the studied sandstones has the comparable geological history, structure, including multiple episodes of magmatic activity to the Taimyr region and Severnaya Zemlya archipelago, and propose that these crustal domain stretch across the Kara Sea, forming the basement to the east and north of FJL, representing the main proximal provenance for the studied Mesozoic clastics. The comparison of the results of the U-Pb dating of rutile, U-Th/He, and U-Pb dating of detrital rutiles are the powerful toll in provenance restoration and can give additional constrains when the provenance area locates within collisional-convergent settings. Moreover, low-temperature thermochronology is necessary for revealing exhumation of the provenance area in intracratonic orogen settings.

Supplementary Materials: The following supporting information can be downloaded at: <https://www.mdpi.com/article/10.3390/geosciences14020041/s1>, Table S1. Results of U-Pb dating of detrital rutiles. Table S2. Trace element concentrations.

Author Contributions: Conceptualization, V.E. and A.P.; methodology, V.E.; formal analysis, V.E. and D.S.; investigation, V.E., A.P. and D.S.; writing—original draft preparation V.E., A.P. and D.S. All authors have read and agreed to the published version of the manuscript.

Funding: Mesozoic stratigraphic and paleogeographic study were supported by RSF grant 21-17-00245. Interpretation of isotopic study and correlation with Taimyr-Severnaya Zemlya were supported by RSF grant 20-17-00169. Field work of AP partly supported by DPMGI SB RAS (FUFG-2024-0005).

Data Availability Statement: The original contributions presented in the study are included in the supplementary material, further inquiries can be directed to the corresponding author.

Acknowledgments: We thank two anonymous reviewers for their constructive comments, suggestions, and corrections, which very much helped to improve the manuscript. Thanks to James Barnett for editing English.

Conflicts of Interest: The authors declare no conflicts of interest.

References

1. Galloway, W.E.; Hobday, D.K. *Terrigenous Clastic Depositional Systems*; Springer: New York, NY, USA, 1983; ISBN 978-1-4684-0172-1.
2. Pettijohn, F.J.; Potter, P.E.; Siever, R. *Sand and Sandstone*; Springer: New York, NY, USA, 1987; ISBN 978-0-387-96350-.
3. Jamil, M.; Siddiqui, N.A.; Ahmed, N.; Usman, M.; Umar, M.; Rahim, H.U.; Imran, Q.S. Facies Analysis and Sedimentary Architecture of Hybrid Event Beds in Submarine Lobes: Insights from the Crocker Fan, NW Borneo, Malaysia. *JMSE* **2021**, *9*, 1133. [[CrossRef](#)]
4. Cawood, P.A.; Hawkesworth, C.J.; Dhuime, B. Detrital Zircon Record and Tectonic Setting. *Geology* **2012**, *40*, 875–878. [[CrossRef](#)]
5. Fedo, C.M.; Sircombe, K.N.; Rainbird, R.H. Detrital Zircon Analysis of the Sedimentary Record. In *Zircon*; Hanchar, J.M., Hoskin, P.W.O., Eds.; De Gruyter: Berlin, Germany, 2003; pp. 277–304, ISBN 978-1-5015-0932-2.
6. Gehrels, G. Detrital Zircon U-Pb Geochronology: Current Methods and New Opportunities. In *Tectonics of Sedimentary Basins*; Busby, C., Azor, A., Eds.; John Wiley & Sons, Ltd.: Chichester, UK, 2012; pp. 45–62. [[CrossRef](#)]
7. Hadlari, T.; Swindles, G.T.; Galloway, J.M.; Bell, K.M.; Sulphur, K.C.; Heaman, L.M.; Beranek, L.P.; Fallas, K.M. 1.8 Billion Years of Detrital Zircon Recycling Calibrates a Refractory Part of Earth’s Sedimentary Cycle. *PLoS ONE* **2015**, *10*, e0144727. [[CrossRef](#)] [[PubMed](#)]
8. Verhaegen, J.; Von Eynatten, H.; Dunkl, I.; Weltje, G.J. Detrital Zircon Geochronology and Heavy Mineral Analysis as Complementary Provenance Tools in the Presence of Extensive Weathering, Reworking and Recycling: The Neogene of the Southern North Sea Basin. *Geol. Mag.* **2021**, *158*, 1572–1584. [[CrossRef](#)]
9. Schwartz, T.M.; Schwartz, R.K.; Weislogel, A.L. Orogenic Recycling of Detrital Zircons Characterizes Age Distributions of North American Cordilleran Strata. *Tectonics* **2019**, *38*, 4320–4334. [[CrossRef](#)]
10. Dickinson, W.R.; Lawton, T.F.; Gehrels, G.E. Recycling Detrital Zircons: A Case Study from the Cretaceous Bisbee Group of Southern Arizona. *Geology* **2009**, *37*, 503–506. [[CrossRef](#)]
11. Andersen, T.; Van Niekerk, H.; Elburg, M.A. Detrital Zircon in an Active Sedimentary Recycling System: Challenging the ‘Source-to-sink’ Approach to Zircon-based Provenance Analysis. *Sedimentology* **2022**, *69*, 2436–2462. [[CrossRef](#)]
12. Burnham, A.D. Zircon. In *Reference Module in Earth Systems and Environmental Sciences*; Elsevier: Amsterdam, The Netherlands, 2018; p. B978012409548910911X. ISBN 978-0-12-409548-9.
13. Chew, D.M.; Sylvester, P.J.; Tubrett, M.N. U–Pb and Th–Pb Dating of Apatite by LA-ICPMS. *Chem. Geol.* **2011**, *280*, 200–216. [[CrossRef](#)]
14. Gaschnig, R.M. Benefits of a Multiproxy Approach to Detrital Mineral Provenance Analysis: An Example from the Merrimack River, New England, USA. *Geochem. Geophys. Geosyst.* **2019**, *20*, 1557–1573. [[CrossRef](#)]
15. Zack, T.; Stockli, D.F.; Luvizotto, G.L.; Barth, M.G.; Belousova, E.; Wolfe, M.R.; Hinton, R.W. In situ U–Pb rutile dating by LA-ICP-MS: ²⁰⁸Pb correction and prospects for geological applications. *Contrib. Mineral. Petrol.* **2011**, *162*, 515–530. [[CrossRef](#)]
16. Zack, T.; Kronz, A.; Foley, S.F.; Rivers, T. Trace element abundances in rutiles from eclogites and associated garnet mica schists. *Chem. Geol.* **2002**, *184*, 97–122. [[CrossRef](#)]
17. Triebold, S.; von Eynatten, H.; Zack, T. A recipe for the use of rutile in sedimentary provenance analysis. *Sediment. Geol.* **2012**, *282*, 268–275. [[CrossRef](#)]
18. Meinhold, G. Rutile and Its Applications in Earth Sciences. *Earth-Sci. Rev.* **2010**, *102*, 1–28. [[CrossRef](#)]
19. Okay, N.; Zack, T.; Okay, A.I.; Barth, M. Sinistral Transport along the Trans-European Suture Zone: Detrital Zircon–Rutile Geochronology and Sandstone Petrography from the Carboniferous Flysch of the Pontides. *Geol. Mag.* **2011**, *148*, 380–403. [[CrossRef](#)]
20. Cherniak, D.J. Pb Diffusion in Rutile. *Contrib. Miner. Petrol.* **2000**, *139*, 198–207. [[CrossRef](#)]

21. Vry, J.K.; Baker, J.A. LA-MC-ICPMS Pb–Pb Dating of Rutile from Slowly Cooled Granulites: Confirmation of the High Closure Temperature for Pb Diffusion in Rutile. *Geochim. Cosmochim. Acta* **2006**, *70*, 1807–1820. [[CrossRef](#)]
22. Pereira, I.; Storey, C.D. Detrital rutile: Records of the deep crust, ores and fluids. *Lithos* **2023**, *438–439*, 107010. [[CrossRef](#)]
23. Thomsen, T.B.; Knudsen, C.; Hinchey, A.M. Investigations of Detrital Zircon, Rutile and Titanite from Present-Day Labrador Drainage Basins: Fingerprinting the Grenvillean Front. *GEUS Bull.* **2015**, *33*, 77–80. [[CrossRef](#)]
24. Pereira, I.; Storey, C.D.; Strachan, R.A.; Bento Dos Santos, T.; Darling, J.R. Detrital rutile ages can deduce the tectonic setting of sedimentary basins. *Earth Planet. Sci. Lett.* **2020**, *537*, 116193. [[CrossRef](#)]
25. Rösel, D.; Zack, T.; Möller, A. Interpretation and Significance of Combined Trace Element and U–Pb Isotopic Data of Detrital Rutile: A Case Study from Late Ordovician Sedimentary Rocks of Saxo-Thuringia, Germany. *Int. J. Earth Sci.* **2019**, *108*, 1–25. [[CrossRef](#)]
26. Kotowski, J.; Nejbort, K.; Olszewska-Nejbort, D. Rutile Mineral Chemistry and Zr-in-Rutile Thermometry in Provenance Study of Albian (Uppermost Lower Cretaceous) Terrigenous Quartz Sands and Sandstones in Southern Extra-Carpathian Poland. *Minerals* **2021**, *11*, 553. [[CrossRef](#)]
27. Bracciali, L.; Najman, Y.; Parrish, R.R.; Akhter, S.H.; Millar, I. The Brahmaputra Tale of Tectonics and Erosion: Early Miocene River Capture in the Eastern Himalaya. *Earth Planet. Sci. Lett.* **2015**, *415*, 25–37. [[CrossRef](#)]
28. Bracciali, L.; Parrish, R.R.; Najman, Y.; Smye, A.; Carter, A.; Wijbrans, J.R. Plio-Pleistocene Exhumation of the Eastern Himalayan Syntaxis and Its Domal ‘Pop-Up’. *Earth-Sci. Rev.* **2016**, *160*, 350–385. [[CrossRef](#)]
29. Drachev, S.S. Fold Belts and Sedimentary Basins of the Eurasian Arctic. *Arktos* **2016**, *2*, 21. [[CrossRef](#)]
30. Drachev, S.S.; Malyshev, N.A.; Nikishin, A.M. Tectonic History and Petroleum Geology of the Russian Arctic Shelves: An Overview. In *Geological Society, London, Petroleum Geology Conference Series*; The Geological Society of London: London, UK, 2010; Volume 7, pp. 591–619. [[CrossRef](#)]
31. Henriksen, E.; Ryseth, A.E.; Larssen, G.B.; Heide, T.; Rønning, K.; Sollid, K.; Stoupakova, A.V. Chapter 10. Tectonostratigraphy of the Greater Barents Sea: Implications for Petroleum Systems. *Geol. Soc. Lond. Mem.* **2011**, *35*, 163–195. [[CrossRef](#)]
32. Pease, V.; Drachev, S.; Stephenson, R.; Zhang, X. Arctic Lithosphere—A Review. *Tectonophysics* **2014**, *628*, 1–25. [[CrossRef](#)]
33. Dibner, V.D. (Ed.) *Geology of Franz Josef Land*; Nor. Polarinst. Meddelelser: Tromsø, Norway, 1998; Volume 146, 199p.
34. Gramberg, I.S.; Shkola, I.V.; Bro, E.G.; Shekhodanov, V.A.; Armishev, A.M. Parametric Wells on the Islands of the Barents and Kara Seas. *Sov. Geol.* **1985**, *1*, 95–98. (In Russian)
35. Makariev, A.A. (Ed.) *State Geological Map of the Russian Federation. Scale 1: 1,000,000 (New Series). Sheet U-37-40—Franz Josef Land (Northern Islands). Explanatory Letter*; Publishing House of VSEGEI: Saint Petersburg, Russia, 2006; 272p. (In Russian)
36. Ershova, V.; Prokopiev, A.; Stockli, D.; Kurapov, M.; Kosteva, N.; Rogov, M.; Khudoley, A.; Petrov, E.O. Provenance of the Mesozoic succession of Franz Josef Land (north-eastern Barents Sea): Paleogeographic and tectonic implications for the High Arctic. *Tectonics* **2022**, *41*, e2022TC007348. [[CrossRef](#)]
37. Corfu, F.; Polteau, S.; Planke, S.; Faleide, J.I.; Svensen, H.; Zayoncheck, A.; Stolbov, N. U–Pb Geochronology of Cretaceous Magmatism on Svalbard and Franz Josef Land, Barents Sea Large Igneous Province. *Geol. Mag.* **2013**, *150*, 1127–1135. [[CrossRef](#)]
38. Senger, K.; Tveranger, J.; Ogata, K.; Braathen, A.; Planke, S. Late Mesozoic Magmatism in Svalbard: A Review. *Earth-Sci. Rev.* **2014**, *139*, 123–144. [[CrossRef](#)]
39. Levskii, L.K.; Stolbov, N.M.; Bogomolov, E.S.; Vasil’eva, I.M.; Makar’eva, E.M. Sr-Nd-Pb Isotopic Systems in Basalts of the Franz Josef Land Archipelago. *Geochem. Int.* **2006**, *44*, 327–337. [[CrossRef](#)]
40. Makariev, A.A. (Ed.) *State Geological Map of the Russian Federation. Scale 1: 1000 000 (Third Generation). Series North-Karsko-Barents Sea. Sheet U-41-44-Franz Josef Land (Eastern Islands). Explanatory Note*; Publishing House of VSEGEI: Saint Petersburg, Russia, 2011; 220p. (In Russian)
41. Kosteva, N.N. Stratigraphy of Jurassic–Cretaceous deposits of Franz Joseph Land. *Arctica Antarct.* **2005**, *4*, 16–32.
42. Repin, Y.S.; Fedorova, A.A.; Bystrova, V.V.; Kulikova, N.K.; Polubotko, I.V. Mesozoic strata of Barents Sea sedimentary basin. In *Stratigraphy and Its Role in Develop of Oil and Gas Complex of Russia*; VNIGRII: Saint Petersburg, Russia, 2007; pp. 112–137. (In Russian)
43. Abashev, V.V.; Metelkin, D.V.; Vernikovskiy, V.A.; Vasyukova, E.A.; Mikhaltsov, N.E. Early Cretaceous Basalts of the Franz Josef Land Archipelago: Correspondence of New $^{40}\text{Ar}/^{39}\text{Ar}$ and Paleomagnetic Data. *Dokl. Earth Sci.* **2020**, *493*, 495–498. [[CrossRef](#)]
44. Grachev, A.F. A new view on the origin of magmatism of the Franz Joseph Land. *Izvestiya Phys. Solid Earth* **2001**, *9*, 49–61.
45. Karyakin, Y.V.; Sklyarov, E.V.; Travin, A.V. Plume Magmatism at Franz Josef Land. *Petrology* **2021**, *29*, 528–560. [[CrossRef](#)]
46. Koryakin, Y.V.; Shipilov, E.V. Geochemical Specifics and $^{40}\text{Ar}/^{39}\text{Ar}$ Age of the Basaltoid Magmatism of the Alexander Land, Northbrook, Hooker, and Hayes Islands (Franz Josef Land Archipelago). *Dokl. Earth Sci.* **2009**, *425*, 260–263. [[CrossRef](#)]
47. Shipilov, E.V.; Karyakin, Y.V. Dikes of Hayes Island (Franz Josef Land Archipelago): Tectonic Position and Geodynamic Interpretation. *Dokl. Earth Sci.* **2014**, *457*, 814–818. [[CrossRef](#)]
48. Luvizotto, G.L.; Zack, T.; Meyer, H.P.; Ludwig, T.; Triebold, S.; Kronz, A.; Münker, C.; Stockli, D.F.; Prowatke, S.; Klemme, S.; et al. Rutile crystals as potential trace element and isotope mineral standards for microanalysis. *Chem. Geol.* **2009**, *261*, 346–369. [[CrossRef](#)]
49. Ludwig, K.R. *Isoplot 3.00: A Geochronological Toolkit for Microsoft Excel*; Berkeley Geochronology Center: Berkeley, CA, USA, 2003; Volume 70.

50. Paton, C.; Hellstrom, J.; Paul, B.; Woodhead, J.; Hergt, J. Iolite: Freeware for the visualisation and processing of mass spectrometric data. *J. Anal. At. Spectrom.* **2011**, *26*, 2508. [CrossRef]
51. Petrus, J.A.; Kamber, B.S. VizualAge: A Novel Approach to Laser Ablation ICP-MS U-Pb Geochronology Data Reduction. *Geostand. Geoanal. Res.* **2012**, *36*, 247–270. [CrossRef]
52. Stacey, J.S.; Kramers, J.D. Approximation of terrestrial lead isotope evolution by a two-stage model. *Earth Planet. Sci. Lett.* **1975**, *26*, 207–221. [CrossRef]
53. Tomkins, H.S.; Powell, R.; Ellis, D.J. The pressure dependence of the zirconium-in-rutile thermometer. *J. Metamorph. Geol.* **2007**, *25*, 703–713. [CrossRef]
54. Bucher, K.; Grapes, R. *Petrogenesis of Metamorphic Rocks*; Springer: Berlin/Heidelberg, Germany, 2011; ISBN 978-3-540-74168-8.
55. Andersson, U.B.; Sjöström, H.; Högdahl, K.H.O.; Eklund, O. The Transscandinavian Igneous Belt, evolutionary models. In *The Transscandinavian Igneous Belt (TIB) in Sweden: A Review of Its Character and Evolution*; Special Paper; Geological Survey of Finland: Espoo, Finland, 2004; Volume 37, pp. 104–112.
56. Bogdanova, S.V.; Bingen, B.; Gorbatshev, R.; Kheraskova, T.N.; Kozlov, V.I.; Puchkov, V.N.; Volozh, Y.A. The East European Craton (Baltica) before and during the Assembly of Rodinia. *Precamb. Res.* **2008**, *160*, 23–45. [CrossRef]
57. Gorbatshev, R. The Transscandinavian Igneous Belt—Introduction and background. In *The Transscandinavian Igneous Belt (TIB) in Sweden: A Review of Its Character and Evolution*; Special Paper; Geological Survey of Finland: Espoo, Finland, 2004; Volume 37, pp. 9–15.
58. Korja, A.; Lahtinen, R.; Nironen, M. The Svecofennian Orogen: A Collage of Microcontinents and Island Arcs. *Geol. Soc. Lond. Mem.* **2006**, *32*, 561–578. [CrossRef]
59. Gee, D.G.; Pease, V. The Neoproterozoic Timanide Orogen of Eastern Baltica: Introduction. *Geol. Soc. Lond. Mem.* **2004**, *30*, 1–3. [CrossRef]
60. Kuznetsov, N.; Soboleva, A.; Udoratina, O.; Hertseva, M.; Andreichev, V. Pre-Ordovician Tectonic Evolution and Volcano–Plutonic Associations of the Timanides and Northern Pre-Uralides, Northeast Part of the East European Craton. *Gondwana Res.* **2007**, *12*, 305–323. [CrossRef]
61. Lorenz, H.; Gee, D.G.; Whitehouse, M.J. New Geochronological Data on Palaeozoic Igneous Activity and Deformation in the Severnaya Zemlya Archipelago, Russia, and Implications for the Development of the Eurasian Arctic Margin. *Geol. Mag.* **2007**, *144*, 105–125. [CrossRef]
62. Prokopiev, A.V.; Ershova, V.B.; Sobolev, N.N.; Korago, E.; Petrov, E.; Khudoley, A.K. New Data on Geochemistry, Age and Geodynamic Settings of Felsic and Mafic Magmatism of the Northeastern Part of October Revolution Island (Severnaya Zemlya Archipelago). AGU Chapman Conference on «Large-Scale Volcanism in the Arctic: The Role of the Mantle and Tectonics». Selfoss, Iceland. 2019. Available online: https://higherlogicdownload.s3.amazonaws.com/AGU/181026d4-2440-440a-a114-8fcd2fc3ada8/UploadedImages/Chapmans/Arctic_Volcanism/ChapmanPresentedAbstracts_ArcticVolcanism.pdf (accessed on 1 October 2023).
63. Kurapov, M.; Ershova, V.; Khudoley, A.; Makariev, A.; Makarieva, E. The First Evidence of Late Ordovician Magmatism of the October Revolution Island (Severnaya Zemlya Archipelago, Russian High Arctic): Geochronology, Geochemistry and Geodynamic Settings. *NJG* **2020**, *100*, 1–15. [CrossRef]
64. Pogrebitskii, Y.E. (Ed.) Novaya Zemlya and Vaygach Island. In *Geological Structure and Mineralogy*; VNIIOkeangeologiya: St. Petersburg, Russia, 2004; 174p.
65. Ershova, V.; Anfinson, O.; Prokopiev, A.; Khudoley, A.; Stockli, D.; Faleide, J.I.; Gaina, C.; Malyshev, N. Detrital Zircon (U-Th)/He Ages from Paleozoic Strata of the Severnaya Zemlya Archipelago: Deciphering Multiple Episodes of Paleozoic Tectonic Evolution within the Russian High Arctic. *J. Geodyn.* **2018**, *119*, 210–220. [CrossRef]
66. Brown, D.; Spadea, P.; Puchkov, V.; Alvarez-Marron, J.; Herrington, R.; Willner, A.P.; Hetzel, R.; Gorozhanina, Y.; Juhlin, C. Arc–Continent Collision in the Southern Urals. *Earth-Sci. Rev.* **2006**, *79*, 261–287. [CrossRef]
67. Puchkov, V.N. The Evolution of the Uralian Orogen. *Geol. Soc. Lond. Spec. Publ.* **2009**, *327*, 161–195. [CrossRef]
68. Zonenshain, L.P.; Kuz'min, M.I.; Natapov, L.M. *Plate Tectonics of the USSR Territory: A Plate Tectonic Synthesis*; Geodynamics Series; American Geophysical Union: Washington, DC, USA, 1990.
69. Scott, R.A.; Howard, J.P.; Guo, L.; Schekoldin, R.; Pease, V. Offset and Curvature of the Novaya Zemlya Fold-and-Thrust Belt, Arctic Russia. In *Geological Society, London, Petroleum Geology Conference Series*; The Geological Society of London: London, UK, 2010; Volume 7, pp. 645–657. [CrossRef]
70. Şengör, A.M.C.; Natal'In, B.A.; Burtman, V.S. Evolution of the Altaid Tectonic Collage and Palaeozoic Crustal Growth in Eurasia. *Nature* **1993**, *364*, 299–307. [CrossRef]
71. Kurapov, M.; Ershova, V.; Khudoley, A.; Luchitskaya, M.; Makariev, A.; Makarieva, E.; Vishnevskaya, I. Late Palaeozoic Magmatism of Northern Taimyr: New Insights into the Tectonic Evolution of the Russian High Arctic. *Int. Geol. Rev.* **2021**, *63*, 1990–2012. [CrossRef]
72. Vernikovskiy, V.; Vernikovskaya, A.; Proskurnin, V.; Matushkin, N.; Proskurnina, M.; Kadilnikov, P.; Larionov, A.; Travin, A. Late Paleozoic–Early Mesozoic Granite Magmatism on the Arctic Margin of the Siberian Craton during the Kara–Siberia Oblique Collision and Plume Events. *Minerals* **2020**, *10*, 571. [CrossRef]
73. Bracciali, L. Coupled Zircon–Rutile U–Pb Chronology: LA ICP–MS Dating, Geological Significance and Applications to Sediment Provenance in the Eastern Himalayan–Indo–Burman Region. *Geosciences* **2019**, *9*, 467. [CrossRef]

74. Mueller, M.A.; Licht, A.; Möller, A.; Condit, C.B.; Fosdick, J.C.; Ocakoğlu, F.; Campbell, C. An Expanded Workflow for Detrital Rutile Provenance Studies: An Application from the Neotethys Orogen in Anatolia; Geochronological data analysis/statistics/modelling. *EGUsphere* **2023**, preprint. [[CrossRef](#)]
75. Rösel, D.; Boger, S.D.; Möller, A.; Gaitzsch, B.; Barth, M.; Oalmann, J.; Zack, T. Indo-Antarctic derived detritus on the northern margin of Gondwana. Evidence for continental-scale sediment transport. *Terra Nova* **2014**, *26*, 64–71. [[CrossRef](#)]
76. Rösel, D.; Zack, T.; Boger, S.D. LA–ICP–MS U–Pb dating of detrital rutile and zircon from the Reynolds Range. A window into the Palaeoproterozoic tectonosedimentary evolution of the North Australian Craton. *Precambrian Res.* **2014**, *255*, 381–400. [[CrossRef](#)]
77. Avigad, D.; Morag, N.; Abbo, A.; Gerdes, A. Detrital Rutile U–Pb Perspective on the Origin of the Great Cambro-Ordovician Sandstone of North Gondwana and Its Linkage to Orogeny. *Gondwana Res.* **2017**, *51*, 17–29. [[CrossRef](#)]
78. Allen, C.M.; Campbell, I.H. Spot dating of detrital rutile by LA–Q–ICP–MS: A powerful provenance tool. In *GSA Denver Annual Meeting, Abstract Paper*; The Geological Society of America (GSA): Boulder, CO, USA, 2007; pp. 196–212.
79. Small, D.; Parrish, R.R.; Austin, W.E.N.; Cawood, P.A.; Rinterknecht, V. Provenance of North Atlantic Ice-Rafted Debris during the Last Deglaciation—A New Application of U–Pb Rutile and Zircon Geochronology. *Geology* **2013**, *41*, 155–158. [[CrossRef](#)]
80. Zack, T.; Von Eynatten, H.; Kronz, A. Rutile Geochemistry and Its Potential Use in Quantitative Provenance Studies. *Sediment. Geol.* **2004**, *171*, 37–58. [[CrossRef](#)]
81. Khudoley, A.K.; Verzhbitsky, V.E.; Zastrozhnov, D.A.; O’Sullivan, P.; Ershova, V.B.; Proskurnin, V.F.; Tuchkova, M.I.; Rogov, M.A.; Kyser, T.K.; Malyshev, S.V.; et al. Late Paleozoic—Mesozoic Tectonic Evolution of the Eastern Taimyr-Severnaya Zemlya Fold and Thrust Belt and Adjoining Yenisey-Khatanga Depression. *J. Geodyn.* **2018**, *119*, 221–241. [[CrossRef](#)]
82. Raimondo, T.; Hand, M.; Collins, W.J. Compressional Intracontinental Orogens: Ancient and Modern Perspectives. *Earth-Sci. Rev.* **2014**, *130*, 128–153. [[CrossRef](#)]

Disclaimer/Publisher’s Note: The statements, opinions and data contained in all publications are solely those of the individual author(s) and contributor(s) and not of MDPI and/or the editor(s). MDPI and/or the editor(s) disclaim responsibility for any injury to people or property resulting from any ideas, methods, instructions or products referred to in the content.